

Politecnico di Torino

Master Degree in Physics of Complex Systems

Stochastic transport of interacting particles: a heterogeneous 1-dimensional model



**Politecnico
di Torino**

SUPERVISORS

Alessandro Pelizzola

Marco Pretti

AUTHOR

Beatrice Mina

Academic Year 2021/2022

Contents

1	Introduction	1
2	Models	3
2.1	TASEP with open boundary conditions	3
2.2	TASEP with periodic boundary conditions	4
3	Methods	6
3.1	Mean field	6
3.2	Cluster mean field: pair approximation	7
3.3	Kinetic Monte Carlo	9
4	Results	11
4.1	Features of the steady state when the interaction is weak	11
4.2	Features of the steady state when the interaction is strong	17
4.3	Steady state particle current and comparison with analytical solutions . . .	21
4.3.1	Weak interaction	23
4.3.2	Strong interaction	25
5	Conclusions and open questions	28

1 Introduction

The majority of physical phenomena that closely affect our lives are out of equilibrium processes, for instance think about vehicular flow, electrical and biological transport.

This thesis concerns a model developed to deal with biological transport which will be treated by means of statistical mechanics in the next Chapters.

We are interested into the steady state of our out of equilibrium system, whose feature is that the variables characterizing the process stay constant in time.

Unlike in equilibrium statistical mechanics, we still do not have a well established theory to study, in the statistical mechanic framework, stationary states of out of equilibrium systems.

Some simple models - that retain only key aspects of the processes taking place in such complex systems - have been proposed, one of them is the so called TASEP and it shows interesting phenomena when investigating multi-particle non-equilibrium systems.

TASEP is the acronym of Totally Asymmetric Simple Exclusion Process and it is regarded as a paradigmatic model for non-equilibrium statistical mechanics, similarly to the role the Ising model plays for equilibrium statistical mechanics. TASEP was firstly proposed as a stochastic model for the kinetics of protein synthesis from mRNA via the polyribosome (see Figure 1).

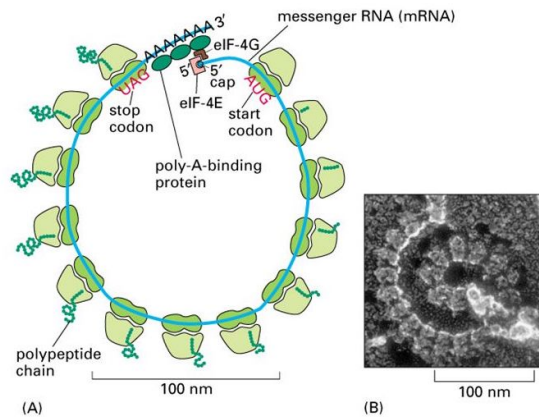


Figure 6-75. Molecular Biology of the Cell, 4th Edition.

Figure 1: (A) Set of ribosomes constituting a polyribosome and simultaneously translating the same mRNA molecule. (From B. Alberts, A. Johnson, J. Lewis, M. Raff, K. Roberts, and P. Walter, *Molecular biology of the cell, 4th edition*, Fig. 6-75) (B) Polyribosome seen under electron microscope. (Photo by John Heuser)

The polyribosome is a set of ribosomes that bind to the same mRNA molecule, each ribosome is a macromolecular complex that works as a molecular motor. Molecular motors convert chemical energy into mechanical energy required for their movement, the mentioned chemical energy is the one released from ATP consumption, reaction that drives the system out of equilibrium.

Ribosomes bind to a well defined codon (which corresponds to each group of three consecutive nucleotides) called starting codon, then they move along the molecule always in the same direction, translating each codon into an amino acid. Those molecular motors can move to the next codon, once the previous one has been translated, only if there is enough space for the ribosome to fit in.

Hence the key aspects of the ribosome kinetics are:

- They are involved into a biological transport process called traffic-like motion which differs from all the other kinds of motion since the motors move along tracks (also called trails) [1]
- Ribosome-mRNA coupling can only occur in a limited region identified as a codon, which can be viewed as a lattice site
- Molecular machines can move only observing excluded volume principle

All the above features can be captured by TASEP model, which is indeed defined over a 1D lattice made of L sites, in which particles can hop, one at a time, only in one direction (as the words "totally asymmetric" in the acronym suggest), say rightward, from one site to its nearest neighbour, if the latter is empty (here is why it is called "simple exclusion process").

Remaining in the biological field, TASEP can also be implemented to mimic the motion of kinesin and dynein, which are protein motors that "walk" along microtubules carrying cellular material; or to deal with the movement of myosin along actin filaments responsible for muscle contraction.

Furthermore the model under consideration can address vehicular traffic problems where traffic is treated as a system of interacting particles (the vehicles) driven far from equilibrium.

The aim of this thesis is to investigate the stationary state phases of a system modeled by TASEP, in particular focusing on the particle density and current and their response to changes in some parameters.

We will deal with a TASEP model which has some specific features (that we will describe in the next Chapters) for which an exact solution is not known. Because of this we will implement some approximate methods and numerical simulations to get the results we are interested in.

Let us outline the structure of this thesis, summarizing the content of each chapter:

- In Chapter 2 we define the features of the specific TASEP model we consider in this work, concerning boundary conditions, hopping rates and particle interactions.
- In Chapter 3 we write the equations for the time evolution of the particles density and current and explains how to tackle them with mean field and cluster mean field approximation methods, besides we describe how to create numerical simulations for our problem with kinetic Monte Carlo.
- Chapter 4 shows the particle density and current obtained through the methods listed in the previous point, and studies the phases that characterize the steady state, depending on some parameters.
- in Chapter 5 we briefly summarize the results achieved in this thesis and try to enlarge a bit the scenario.

2 Models

As anticipated in the previous Section, TASEP is defined over a 1D lattice, its nodes are labeled by $i = 0, \dots, L - 1$, and to each of them is associated an occupation number n_i^t , which takes value 0 if that site is empty or 1 if that site is occupied by one particle at time t .

The local density of particles is denoted by $\rho_i^t = \langle n_i^t \rangle$, and corresponds to the ensemble average over all possible realizations of our stochastic process at any time.

TASEP can be characterized by open or periodic boundary conditions (referred to as OBC and PBC respectively) and by uniform or inhomogeneous hopping rates.

In this Section we are going to briefly analyze the case of OBC, whereas we are going to just introduce the features of the model with PBC and then we will discuss it extensively in the next Chapters.

2.1 TASEP with open boundary conditions

We present the simplest case in which hopping rates from site i to $i + 1$, $i \in \{0, \dots, L - 2\}$, are all unitary and stay constant during the time evolution of the system.

Particles are injected in the 1D lattice from the left in site 0 (provided it is empty) with probability rate α , and are extracted from site $L - 1$ on the right (provided it is occupied) with rate β (as illustrated in Figure 2). This situation is equivalent to the one in which the system is assumed to be in contact with 2 reservoirs of fixed densities $\rho_l = \alpha$ and $\rho_r = 1 - \beta$, with $\alpha, \beta \in (0, 1)$, at its leftmost and rightmost nodes respectively.

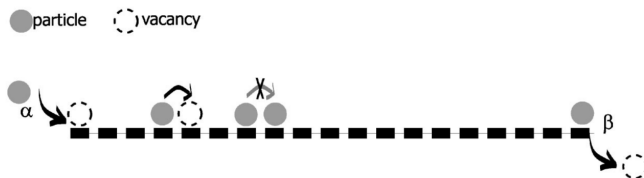


Figure 2: TASEP with open boundary conditions and unitary hopping rates, with injection probability rate α and emission probability rate β . (From H. Hinsch, R. Kouyos, and E. Frey, *From Intracellular Traffic to a Novel Class of Driven Lattice Gas Models*, Fig. 1)

Depending on the values of α and β , the stationary state of the system can belong to 3 different phases, as displayed in Figure 3.

When $\alpha < \beta$ and $\alpha < 1/2$ the phase characterizing the system is the low density (LD) one, that is the bulk (uniform) density is smaller than $1/2$. The value of ρ is the macroscopic result of the behaviour of the system at the boundaries (particles exit faster than they enter).

Conversely if $\beta < \alpha$ and $\beta < 1/2$, the state of the system corresponds to the high density (HD) phase, id est the bulk density is larger than $1/2$.

Eventually setting $\alpha, \beta > 1/2$ the system is found to be in the so called maximal current (MC) phase, represented by a bulk density equal to $1/2$.

Notice that the boundary between high and low density phases is demarcated by the coexistence line ($\alpha = \beta$ with $\alpha, \beta < 1/2$) over which the system displays a linear density profile and the transition between LD phase and HD phase is discontinuous.

Instead the transitions between low or high density phases and maximal current phase are continuous.

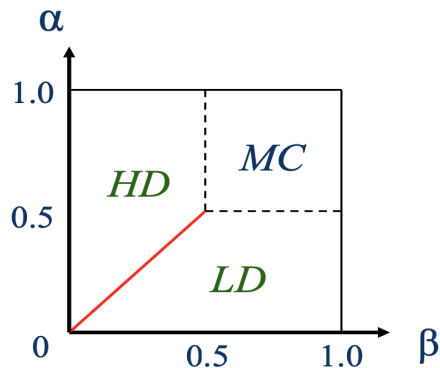


Figure 3: Phase diagram for TASEP with open boundary conditions and unitary hopping rates, (From R.K.P. Zia, J.J. Dong, B. Schmittmann, *Modeling Translation in Protein Synthesis with TASEP: A Tutorial and Recent Developments*, Fig.2)

2.2 TASEP with periodic boundary conditions

The model on which we focus in this thesis is characterized by periodic boundary conditions, i.e. node $L - 1$ and node 0 are adjacent, therefore the 1D lattice is shaped like a ring of L sites in which the number of particles $N = \sum_{i=0}^{L-1} n_i^t$ is conserved at any time t .

Now we want to provide a more general version of the model in order to best suit transport phenomena we talked about in Chapter 1. Quenched hopping rates and interactions between particles are introduced.

Unitary hopping rates are not the best choice to provide a realistic description of biological (or vehicular) transport. Indeed, for instance, when a ribosome is "walking" on mRNA and encounters a turn or an inhomogeneity on its trail, it slows down or speeds up. This behaviour can be modeled by quenched hopping rates, which are referred to as λ_i and have different values from site to site.

Neglecting interactions between particles for now, we assume that the hopping rate from site $i - 1$ to i is $\lambda_i \in [0, 1]$ and is equal to $\lambda(i/L)$ which is piecewise continuous, smooth, slowly varying, has a single point global minimum and its explicit expression is $\lambda(i/L) = ((i + 0.5)/L - 0.5)^2 + 0.5$, for $i = 0, \dots, L - 1$ [2].

Furthermore, since in vehicular traffic a car slows down when approaching the one in front of it and the same is observed in ribosome motion, it makes sense to include nearest neighbour interactions in our model. Taking into account these interactions in our TASEP corresponds to employ hopping rates that are affected by the occupancy of nearest neighbours, hence the quenched hopping rate from site i to $i + 1$ that stands for interacting particles is $\Gamma_{i,i+1}(n_{i-1}, n_{i+2})$ and depends on the occupation numbers of the sites adjacent to the ones involved in the hopping.

We assume that nearest neighbor particles interact through an energy E - associated to the bond between them - which can be attractive or repulsive ($E > 0$ and $E < 0$ respectively). As shown in Figure 4, any time a particle can make a step forward from site $i - 1$ into site i , without changing the total number of bonds, it is characterized by a hopping rate $\Gamma_{i-1,i}(n_{i-2}, n_{i+1}) = \Gamma_{i-1,i}(0, 0) = \Gamma_{i-1,i}(1, 1)$ equal to λ_i .

Instead if the transition to a new state comes with the creation of a new bond, the hopping rate becomes $\Gamma_{i-1,i}(0, 1) = q\lambda_i$; similarly the hopping that determines the breaking

of a bond has a rate $\Gamma_{i-1,i}(1,0) = r\lambda_i$, with $q, r \neq 1$. Creating and breaking the pair of particles can be viewed as opposite chemical reactions, so the detailed balance arguments can be applied obtaining $q/r = e^E$ [3], and one can write the explicit values of the hopping rates

$$q = e^{\Theta E} \quad r = e^{(\Theta-1)E} \quad (1)$$

where Θ ($0 \leq \Theta \leq 1$) can be set equal to $1/2$ if one assumes that the energy E is equally split between creation and breaking processes[3]. The physical meaning of (1) is that when 2 neighboring particles experience an attractive interaction ($E>0$), q is bigger than 1 so the rate related to the bond creation process is larger, while the rate related to bond destruction is smaller; the viceversa happens for $E<0$ [4].

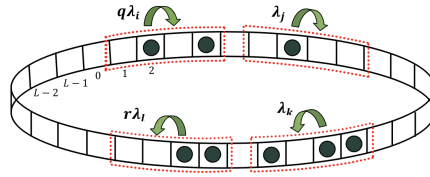


Figure 4: TASEP with periodic boundary conditions and hopping rates as described in the text above (From B. Pal , A. K. Gupta, *Role of interactions in a closed quenched driven diffusive system*, Fig.1)

3 Methods

In this work three techniques have been implemented to study the time evolution of a system modeled by TASEP with quenched hopping rates and local interactions as described in Section 2.2, they are: simple mean field, cluster mean field and kinetic Monte Carlo. All of them aim at working out the behaviour of the particle density and current, and they share some common considerations that we are going to analyze in the following lines.

Let us introduce the current of particles from site i to $i + 1$ at time t , as reported in [5]:

$$J_i^t = \lambda_{i+1} \langle n_i^t (1 - n_{i+1}^t) [(1 - n_{i-1}^t)(1 - n_{i+2}^t) + n_{i-1}^t n_{i+2}^t + rn_{i-1}^t (1 - n_{i+2}^t) + q(1 - n_{i-1}^t) n_{i+2}^t] \rangle \quad (2)$$

This expression contains an ensemble average of the sum of four terms, each of them stands for one possible particle configuration in the nodes involved in the hopping ($n_{i-1}^t, n_i^t, n_{i+1}^t, n_{i+2}^t$ equal to 1 or 0) and it is multiplied by the corresponding hopping rate according to the rules shown at the end of Chapter 2. Notice that the four addends have in common one factor: $n_i^t (1 - n_{i+1}^t)$, meaning that the hopping from node i to $i + 1$ can only occur if the first site is occupied ($n_i^t = 1$) and the latter is empty ($n_{i+1}^t = 0$).

An equivalent description can be provided in terms of joint probabilities (over the same four sites) of having a certain sequence of occupation numbers.

For instance:

$$\langle n_i^t (1 - n_{i+1}^t) (1 - n_{i-1}^t) (1 - n_{i+2}^t) \rangle = P_{i-1}^t [0100] \quad (3)$$

where $P_{i-1}^t [0101]$ is the probability that, at time t , the occupation numbers are $n_{i-1} = 0$, $n_i = 1$, $n_{i+1} = 0$ and $n_{i+2} = 1$.

Hence rewriting (2) in terms of marginal probabilities one obtains:

$$J_i^t = \lambda_{i+1} \left(P_{i-1}^t [0100] + P_{i-1}^t [1101] + r P_{i-1}^t [1100] + q P_{i-1}^t [0101] \right) \quad (4)$$

Recalling that $\Gamma_{i,i+1}(n_{i-1}, n_{i+2})$ are the position dependent hopping rates from site i to $i + 1$:

$$\Gamma_{i,i+1}(1, 1) = \Gamma_{i,i+1}(0, 0) = \lambda_{i+1} \quad (5)$$

$$\Gamma_{i,i+1}(1, 0) = r \lambda_{i+1} \quad (6)$$

$$\Gamma_{i,i+1}(0, 1) = q \lambda_{i+1} \quad (7)$$

we are able to obtain a more compact form for the current expression

$$J_i^t = \sum_{k,n=0,1} P_{i-1}^t [k10n] \Gamma_{i,i+1}(k, n) \quad (8)$$

Four-nodes marginals in the current formula are difficult to handle, so we are going to introduce some approximate methods.

3.1 Mean field

Simple mean field approximation consists in neglecting correlations between particles, so within this approach the four-nodes marginals appearing in (8) are factorizable into single-nodes marginals

$$P_{i-1}^t [n_{i-1} n_i n_{i+1} n_{i+2}] \cong P_{i-1}^t [n_{i-1}] P_i^t [n_i] P_{i+1}^t [n_{i+1}] P_{i+2}^t [n_{i+2}] \quad (9)$$

Now notice that single-node probabilities coincide with ensemble averages, indeed the probability that node $i - 1$ is occupied at time t , is equal to the ensemble average of occupation numbers in $i - 1$ at t , id est $P_{i-1}^t[1] = \langle n_{i-1}^t \rangle$ and then $P_{i-1}^t[0] = \langle 1 - n_{i-1}^t \rangle$. Moreover recalling that $\langle n_{i-1}^t \rangle = \rho_{i-1}^t$, it is possible to establish a well defined connection between probabilities, densities and occupation numbers:

$$P_i^t[1] = \langle n_i^t \rangle = \rho_i^t \quad (10)$$

$$P_i^t[0] = \langle 1 - n_i^t \rangle = 1 - \rho_i^t \quad (11)$$

and formula (8) can be re-expressed as

$$J_i^t \cong \lambda_{i+1} \rho_i^t (1 - \rho_{i+1}^t) \left((1 - \rho_{i-1}^t)(1 - \rho_{i+2}^t) + \rho_{i-1}^t \rho_{i+2}^t + r \rho_{i-1}^t (1 - \rho_{i+2}^t) + q (1 - \rho_{i-1}^t) \rho_{i+2}^t \right) \quad (12)$$

At this point it is possible to know J_i^t and ρ_i^t at any time combining (12) with the continuity equation

$$\dot{\rho}_i^t = J_{i-1}^t - J_i^t \quad (13)$$

Since our aim is to numerically solve (12) and (13) through a computer algorithm that approximates the time evolution of our system, we rewrite (14) in its discretized form:

$$\frac{\rho_i^{t+\Delta} - \rho_i^t}{\Delta} = J_{i-1}^t - J_i^t \quad (14)$$

where Δ is the time difference between 2 consecutive steps. We have selected a value for Δ which is able to balance two opposite requirements: it has to be large enough in order to guarantee a not too long computational time to reach the stationary state and, on the other hand, it has to be small enough to ensure the convergence to the steady state.

The suitable value we have chosen is $\Delta = 0.01$.

The implementation of such algorithm is made up of two main phases:

1. Once fixed N (particle number) and L (site number), $\rho_0^0, \dots, \rho_{L-1}^0$ are all initialized to N/L (uniform density) and the currents (J_i) are consequently determined by (12)

2. Update the densities and currents at each time step until convergence. To determine

when the stationary state is reached we define a parameter $\zeta = \sum_{i=0}^{L-1} \frac{|\rho_i^t - \rho_i^{t-\Delta}|}{L}$, and we stop the algorithm when ζ stays below a certain threshold that we have reasonably identified with 1×10^{-12} .

3.2 Cluster mean field: pair approximation

Mean field cluster approximations are obtained assuming that the only relevant interactions are among clusters of k sites and consequently the probability distribution of the model factors as something proportional to the product of k -sites marginals. Pair approximation belongs to the cluster MF techniques and consists in retaining only correlations between adjacent nodes.

Obviously, for interacting systems like the one under analysis here, numerical results become progressively accurate as cluster size increases, this is the reason why we are moving from a one-site cluster technique (the simple mean field) to a two-site cluster method.

First of all we define the particle current from site i to $i + 1$, a time t , through formula (8), subsequently, since we want to take into account only correlations between adjacent sites, the marginal over 4 nodes can be approximated as the product of marginals over 2 nodes, divided by the product of 2 single-node marginals [6]:

$$P_{i-1}^t[n_{i-1}n_in_{i+1}n_{i+2}] \cong \frac{P_{i-1}^t[n_{i-1}n_i]P_i^t[n_in_{i+1}]P_{i+1}^t[n_{i+1}n_{i+2}]}{P_i^t[n_i]P_{i+1}^t[n_{i+1}]} \quad (15)$$

Then using this approximation to rewrite equation (8), one obtains

$$J_i^t \cong \frac{\lambda_{i+1}P_i^t[10]}{P_i^t[1]P_{i+1}^t[0]} \left(P_{i-1}^t[01]P_{i+1}^t[00] + P_{i-1}^t[11]P_{i+1}^t[01] + rP_{i-1}^t[11]P_{i+1}^t[00] + qP_{i-1}^t[01]P_{i+1}^t[01] \right) \quad (16)$$

Now we would like to express J_i^t as a function of the densities (ρ_i^t). but we only know how to substitute single-node probabilities with densities (through formulas (10) and (11)), whereas in equation (16) appear two-nodes marginals.

Hence we are interested in providing a relation between marginals over one and two nodes, to this aim we can exploit the following marginalization equalities

$$P_i^t[1] = P_i^t[10] + P_i^t[11], \quad P_i^t[0] = P_i^t[01] + P_i^t[00], \quad P_{i+1}^t[1] = P_i^t[01] + P_i^t[11]$$

Then setting $\phi_i^t = P_i^t[11]$, the marginals over 2 nodes appearing in (16) can be expressed as:

$$P_i^t[10] = \rho_i^t - \phi_i^t \quad (17)$$

$$P_i^t[01] = \rho_{i+1}^t - \phi_i^t \quad (18)$$

$$P_i^t[00] = 1 - \rho_i^t - \rho_{i+1}^t + \phi_i^t \quad (19)$$

and eventually one obtains

$$J_i^t \cong \frac{\lambda_{i+1}(\rho_i^t - \phi_i^t)}{\rho_i^t(1 - \rho_{i+1}^t)} [(\rho_i^t - \phi_{i-1}^t)(1 - \rho_{i+1}^t - \rho_{i+2}^t + \phi_{i+1}^t) + \phi_{i-1}^t(\rho_{i+2}^t - \phi_{i+1}^t) + r\phi_{i-1}^t(1 - \rho_{i+1}^t - \rho_{i+2}^t + \phi_{i+1}^t) + q(\rho_i^t - \phi_{i-1}^t)(\rho_{i+2}^t - \phi_{i+1}^t)] \quad (20)$$

Equation (20) with the discretized version of the continuity equation (14) does not form a closed system of equations, therefore it is necessary to investigate the time evolution of ϕ_i^t , for this purpose let us write the master equation provided in [7] and add it to the aforesaid system.

$$\dot{\phi}_i^t = \sum_{k=0,1} P_{i-2}^t[k101]\Gamma_{i-1,i}(k,1) - \sum_{n=0,1} P_i^t[110n]\Gamma_{i+1,i+2}(1,n) \quad (21)$$

The master equation (21) tells us that the probability that i and $i + 1$ are both occupied tends to increase in time if the particle gain term is bigger than the particle loss term; that is if the probability that a particle hops in i , given that $i + 1$ is already occupied (gain) is bigger than the probability that a particle hops in $i + 2$, leaving $i + 1$ empty, provided that i is already occupied (loss).

Applying approximation (15) and formulas from (17) to (19) to equation (21), it becomes

$$\begin{aligned} \dot{\phi}_i^t \simeq & \frac{(\rho_{i-1}^t - \phi_{i-1}^t)(\rho_{i+1}^t - \phi_i^t)\lambda_i}{\rho_{i-1}^t(1 - \rho_i^t)}((\rho_{i-1}^t - \phi_{i-2}^t)q + \phi_{i-2}^t) + \\ & - \frac{\phi_i^t(\rho_{i+1}^t - \phi_{i+1}^t)\lambda_{i+2}}{\rho_{i+1}^t(1 - \rho_{i+2}^t)}((1 - \rho_{i+2}^t - \rho_{i+3}^t + \phi_{i+2}^t)r + (\rho_{i+3}^t - \phi_{i+2}^t)) \end{aligned} \quad (22)$$

Finally we have a closed system of equations composed by (20), (22) and (14) that allows us to study the behaviour of the densities, currents and probabilities of the system under analysis.

The computer algorithm implemented to approximate the time evolution of our model is the same as the one described in the simple mean field case, except for the fact that now also $\phi_0, \dots, \phi_{L-1}$ have to be initialized and updated at each step.

We have chosen $(N/L)^2$ as initial values of ϕ_i for $i = 0, \dots, L-1$, i.e. we have assumed that at the beginning the system does not experience any correlation, indeed $\phi_i^0 = P_i^0$ [11] in mean field approximation is equal to $\rho_i^0 \rho_{i+1}^0 = N/L \times N/L$.

Notice that the choice of the initial conditions does not affect the stationary state since we are dealing with a Markov process, indeed the configuration of the system, the currents and the densities at time t depend only on their values at time $t-1$.

3.3 Kinetic Monte Carlo

This technique is also known as Gillespie algorithm and it aims at simulating the time evolution of a system in a stochastic manner. It is useful to analyze continuous time Markov processes and belongs to Monte Carlo methods, but it does not deal with the master equation directly.

Suppose that the system under analysis is a 1D lattice whose configuration at the initial time $t = 0$ is known. Let's call such initial state $s^0 = (n_0^0, \dots, n_{L-1}^0)$, where $n_i^t \in \{0, 1\}$; then in order to "move the system forward in time" it is sufficient to know the answers to the questions: *when will the next change of configuration occur?* and *what will the new configuration be?*

It is important to notice that in this case the transition to the next state corresponds to the hopping of one single particle from site $i-1$ to i , so the transition rates W_i are equal to the hopping rates $\Gamma_{i-1,i}(n_{i-2}, n_{i+1})$.

The probability that a transition to state $s^{t'}$ occurs in $(t, t+dt)$, given the system is in state s^t at t , is $dtW_{s \rightarrow s'}$, meaning that the probability of the change of configuration corresponding to a particle hopping from site $i-1$ to site i is dtW_i .

Hence the probability that the next transition is the hopping from $i-1$ to i and occurs in the infinitesimal time interval $(t+\tau, t+\tau+d\tau)$, given s^t at t , is $P(\tau, i)d\tau$ which can be written as

$$P(\tau, i)d\tau = P_0(\tau)d\tau W_i \quad (23)$$

where $P_0(\tau)$ is the probability that no transition occurs in $(t, t+\tau)$, with t time of the last transition.

If one splits the interval $(t, t+\tau)$ into n sub-intervals $d\tau = \tau/n$ with $n \rightarrow \infty$, then $P_0(\tau)$ can be obtained as the probability of having 0 "successes" (= no transition) in n "attempts"

(= the n sub-intervals), such probability is given by the product of the probabilities of not having a transition in one attempt:

$$P_0(\tau) = \left(1 - d\tau \sum_{l=0}^{L-1} W_l\right)^n = \left(1 - \frac{\tau}{n} \sum_{l=0}^{L-1} W_l\right)^n \xrightarrow{n \rightarrow \infty} e^{-\tau \sum_{l=0}^{L-1} W_l} \quad (24)$$

Implying that

$$P(\tau, i) = W_i e^{-\tau \sum_{l=0}^{L-1} W_l} \quad (25)$$

At this point, one wants to obtain a random pair (τ, k) from a set described by the probability density $P(\tau, k)$. It is proven that this can be done by taking two random numbers ϵ_1 and ϵ_2 from the unit-interval uniform distribution, and then by computing

$$\tau = -\frac{1}{\sum_{i=0}^{L-1} W_i} \ln(\epsilon_1) \quad (26)$$

$$\sum_{i=0}^{k-1} W_i < \epsilon_2 \sum_{i=0}^{L-1} W_i \leq \sum_{i=0}^k W_i \quad (27)$$

The majority of the above considerations and the proof of the validity of equations (26) and (27) are provided in [8].

The computer algorithm I have implemented in order to simulate the time evolution of the system described in Chapter 1 consists of 3 main steps:

1. Set the initial time t at 0, define a maximum number of transitions $T = 1 \times 10^8$ and randomly assign 0 or 1 to each n_i^0 making sure that $\sum_{i=0}^{L-1} n_i^0 = N$. Assign also the $W_i = \Gamma_{i-1,i}(n_{i-2}, n_{i+1})$.
2. Thanks to (26) it is possible to know the time of the next transition which corresponds to $t + \tau$. Furthermore the site of the ring in which a particle is going to hop corresponds to the k that verifies (27). Note that the formulation itself of (27) is sufficient to guarantee that the hopping occurs from an occupied site to an empty site.
3. After the transition it is necessary to update the occupation numbers of the 2 sites involved in the hopping ($k - 1$ and k), and consequently also the hopping rates referred to the nodes near k . Then the algorithm returns at Point 2 and performs these cyclic operations until the established number of transitions is reached.

In the end the density of particles is computed performing a weighted time average over the occupation numbers obtained after each transition, where the weights are the time intervals between two subsequent transitions

$$\rho_i = \sum_{j=T_0}^{T-1} \frac{n_i^{t_{j+1}}(t_{j+1} - t_j)}{t_{T-1} - t_{T_0}} \quad (28)$$

The sum does not start from the first transition but from the one occurred at time step T_0 , whose value, chosen after proper testing, is set at the 5% of T . This procedure is intended to exclude the transient while computing the densities ρ_i at the steady state.

4 Results

In the following we will portray the behaviour of stationary state density profiles characterizing a system modeled by TASEP with periodic boundary conditions, quenched hopping rates and interactions (as defined in Section 2.2), comparing the pictures provided by mean field, cluster mean field and kinetic Monte Carlo methods.

It is known that in the case of TASEP model with open boundary conditions and no interactions (except for simple exclusion), mean field analysis provides results in very good agreement with the exact ones (see [9]). We wonder whether this is also true in the case with periodic boundary conditions and nearest neighbour interactions.

In general, since we are interested in the properties of our system in the thermodynamic limit, we choose a large number of lattice sites L . During the analysis we will vary the value of L , keeping it large but not big enough to consider the system as if it were in the thermodynamic limit, otherwise the computational effort would be too great and time-consuming. Despite this we will obtain interesting outcomes.

We will consider some fixed values of the interaction energy E , for which qualitatively different phenomenologies will be observed, varying the average density n .

4.1 Features of the steady state when the interaction is weak

Let us start by investigating the relation between the local density of particles and the lattice sites, considering an interaction energy E equal, in absolute value, to 0.8.

To do so we have created 3 computer algorithms - one for each method described in Chapter 3 - that compute the density of particles ρ_i at the steady state.

Suppose that the number of lattice sites L is set at 1000 (we will keep this value constant throughout the whole Section, unless we explicitly indicate a different value), then the number of particles N can be at most equal to L . In this case we have seen, after some attempts, that to reach the steady state, whose achievement has been decided to take place when ζ stays below 1×10^{-12} with MF and CMF (see Section 3.1), it is necessary to let the system evolve for at least $T = 1 \times 10^8$ transitions when implementing KMC.

For instance when we choose $N = 750$, meaning that the average density of particles $n = N/L$ is equal to 0.75, we obtain the profiles $\rho(x)$ shown in Figure 5, in which $x = i/L$, and panels (a) and (b) are obtained for $E = -0.8$ and $E = 0.8$ respectively.

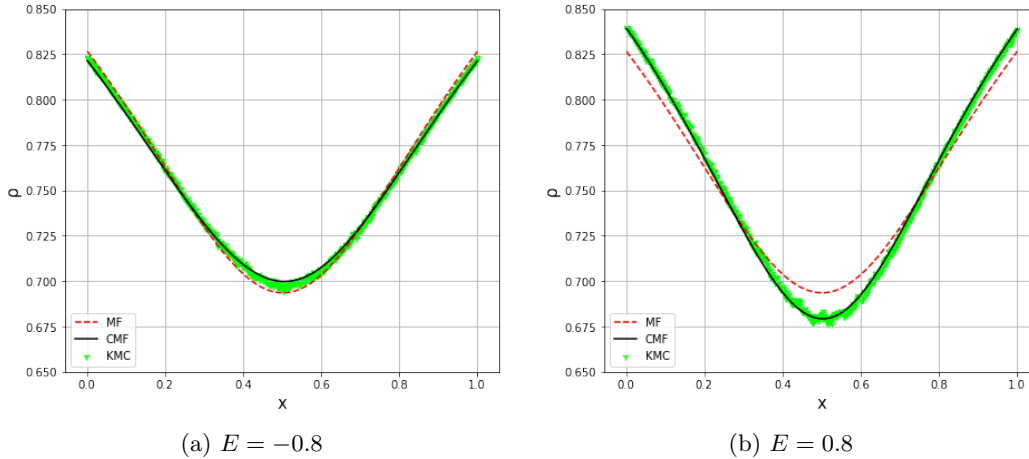


Figure 5: Steady state $\rho(x)$ along a 1D lattice with $L = 1000$ sites, for average density $n = 0.75$ and interaction energy equal to -0.8 in panel (a) and 0.8 in panel (b)

Both for positive and negative energy the values of the density remains well above the intermediate density $\rho = 0.5$, as it happens in the case of TASEP with open boundary when the system is in the high density phase. In our case though, $\rho(x)$ is not constant, so we say that the stationary state of our system corresponds to the generalized high density phase.

The profiles obtained through the three different methods are quite similar, but it is possible to observe that mean field (MF) is not able to distinguish between positive and negative interaction energy. Instead cluster mean field (CMF) is able to predict the correct behaviour obtained through numerical simulations (KMC).

We proceed now showing (Figure 6) the behaviour of the density for $n = 0.25$, keeping unchanged all the other parameters seen in the previous case: $L = 1000$, $|E| = 0.8$. Notice that these profiles are complementary to the ones in Figure 5 due to the particle-hole symmetry.

Again it is observed that MF produces exactly the same density profiles whether the interaction energy is attractive or repulsive, instead CMF reproduces better the results obtained through kinetic Monte Carlo.

In addition let us note that the values of ρ stay always below the intermediate density $\rho = 0.5$, so the phase characterizing the system is the so called generalized low density phase.

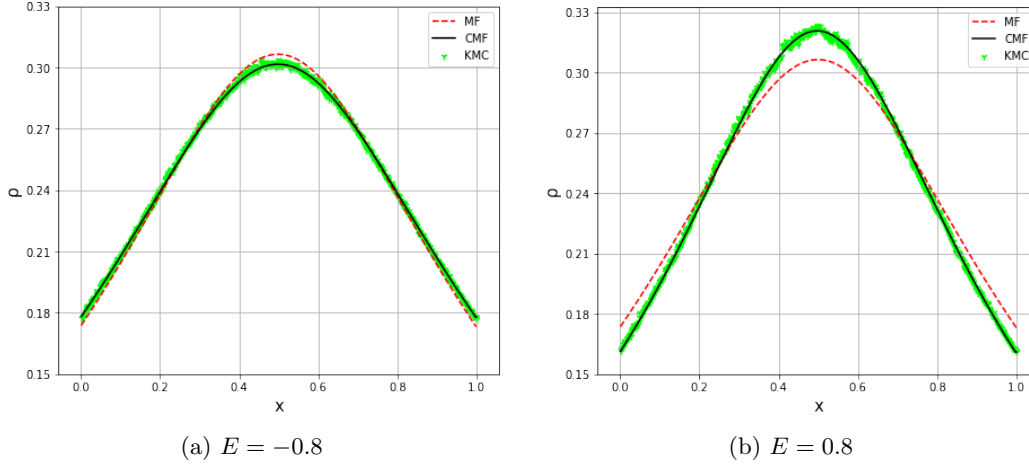


Figure 6: Steady state $\rho(x)$ along a 1D lattice with $L = 1000$ sites, for average density $n = 0.25$ and interaction energy equal to -0.8 in panel (a) and 0.8 in panel (b)

The peculiarity that distinguishes CMF from MF is that, in cluster mean field, the probability of having both site i and $i + 1$ occupied is $P_i[11] = \phi_i$ and it is different from the product of single-node probability of having site i occupied (ρ_i) and independently site $i + 1$ also occupied (ρ_{i+1}); whereas in mean field $P_i[11] = \rho_i\rho_{i+1}$.

In Figure 7 we report the estimated values of ϕ_i and $\rho_i\rho_{i+1}$ computed at the steady state for $i \in \{0, \dots, L - 2\}$, for a system with average density $n = 0.25$ and made of $L = 1000$ sites.

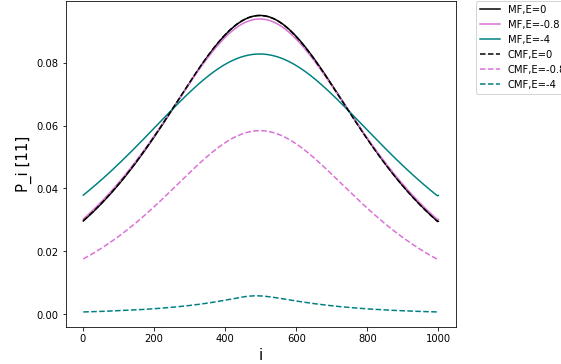


Figure 7: Comparison between $P_i[11]$ determined through MF and CMF for energies equal to 0 and -0.8

In absence of interactions between nearest neighbour particles the mean field and cluster mean field behaviours coincide, as expected. Instead when the energy is slightly below zero, meaning that neighboring particles experience a little repulsion, the effect of this kind of interaction is to lower the probability that two adjacent sites are occupied.

At this point, let us see what happens if we choose an intermediate value for the average density: when $n = 0.6$ and $L = 1000$ the system is found to be in a new phase, with different features with respect to the HD and LD ones, as illustrated in Figure 8 .

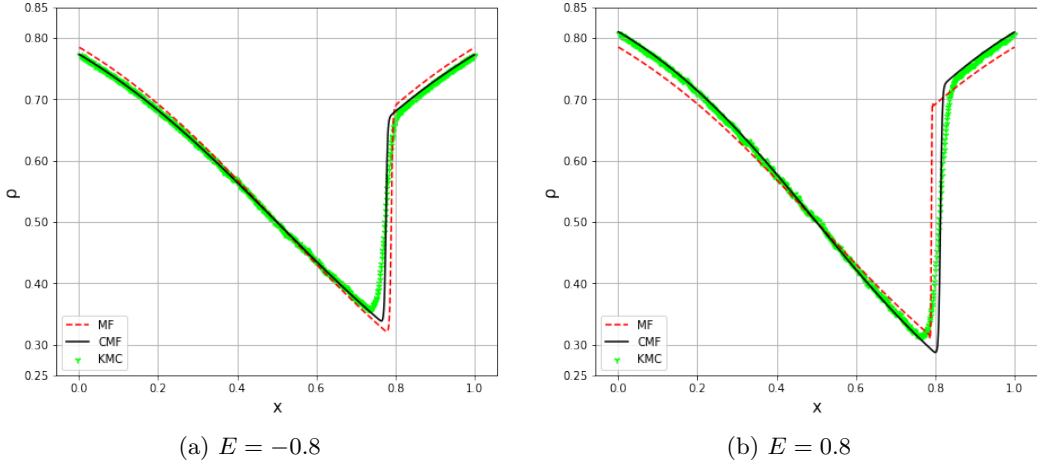


Figure 8: Steady state $\rho(x)$ along a 1D lattice with $L = 1000$ sites, for average density $n = 0.6$ and interaction energy equal to -0.8 in panel (a) and 0.8 in panel (b)

Both for attractive and repulsive interaction, the new phase is characterized by a shock (or domain wall) and for this reason it is called shock phase.

This shock is qualitatively well described by mean field, but the best quantitative description is provided by cluster mean field (for the reasons explained above).

The domain wall corresponds to a jump from a low density value (ρ_b) to a high density value ($\rho_t = 1 - \rho_b$). Little discrepancies with respect to this symmetry, that can be observed in Figure 8, are due to the fact that results are obtained at finite size, that is why the domain wall is not perfectly vertical.

In fact it is possible to verify that both CMF and KMC methods show that the sharpness and steepness of the density profiles increase as the size of the system increases, as displayed in Figure 9; hence the jump becomes a 1st kind discontinuity in the thermodynamic limit.

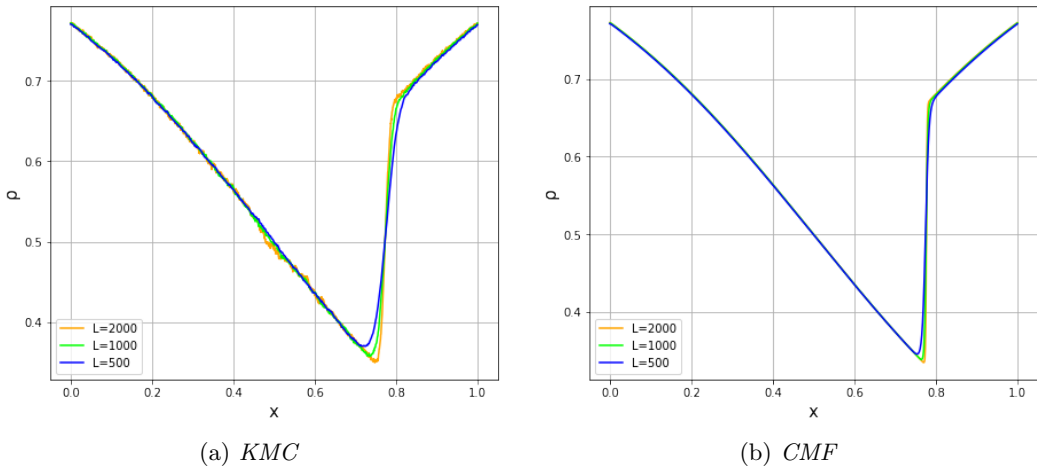


Figure 9: Comparison among $\rho(x)$ profiles obtained by KMC in panel (a) and CMF in panel (b), varying L , for $n = 0.6$ and $E = -0.8$

Furthermore the theoretical predictions and the numerical ones get closer and closer as the size L increases, as reported in Figure 10, meaning that the discrepancies between the theoretical predictions and the numerical simulations are only due to size effects.

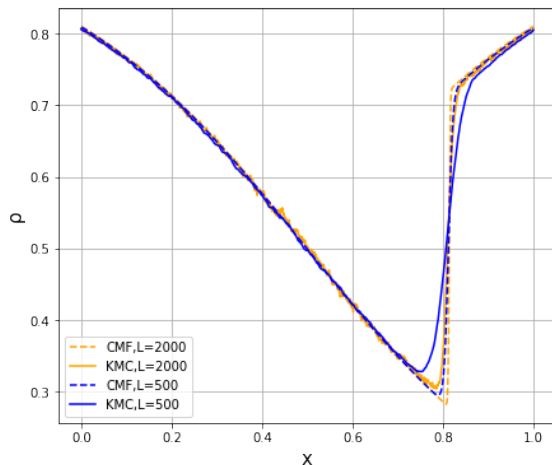


Figure 10: Comparison between $\rho(x)$ profiles provided by CMF and KMC as L varies, for $n = 0.6$ and $E = -0.8$

Let us now describe the features of the transition we have just observed. The behaviour of $\rho(x)$ varies depending on the average density n , but the density profiles for $n < 0.5$ are symmetric to the ones obtained for $n > 0.5$ due to the particle-hole symmetry. (Think about the complementarity of the density profiles in Figures 5 and 6)

For $n \rightarrow 1$, the steady state $\rho(x)$ stays above $1/2 \forall x$, whereas for $n \rightarrow 0$ the stationary density is smaller than $1/2 \forall x$, in both cases the system is said to be in a smooth phase. These smooth phases are characterized by a spatially non-uniform density, so they can be considered a generalization of the uniform high density and low density phases that we have talked about in case of TASEP with open boundary conditions (Section 2.1).

Instead when $n \rightarrow 1/2$, the corresponding $\rho(x)$ has a range of values above $1/2$ and some values below, and presents a jump (domain wall) from values of $\rho(x)$ typical of the LD phase, to values typical of the HD phase. In this case the steady state of the system is called shock phase (see [10]).

Hence there exist 2 critical values of n , in correspondence of which the transitions occur, which are n_{c1} and n_{c2} with $n_{c1} < n_{c2}$. For $n_{c2} < n < 1$ the system is in the HD phase, for $0 < n < n_{c1}$ the state of the system is the LD phase, whereas for $n_{c1} < n < n_{c2}$ the system is characterized by the "coexistence" of the HD and LD phases.

Moreover for n increasing from 0 to 1, the system finds itself firstly in a smooth phase, then in a shock phase and eventually in a smooth phase again, so the non equilibrium phase transitions that occur in this process are called "reentrant" phase transitions [10].

A quite complete picture of what we have just said above is displayed in Figure 11 and is obtained through CMF analysis, for nearest neighbors interaction $E = -0.8$.

Notice that the domain wall in the steady state $\rho(x)$ profiles of the shock phase, moves as n varies; indeed as n approaches $1/2$ from higher values, the position of the shock moves toward $x = 1$.

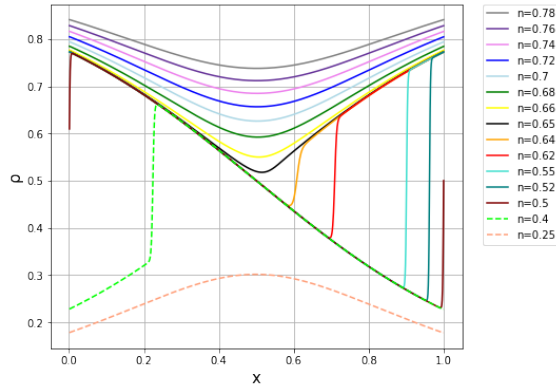


Figure 11: Comparison among $\rho(x)$ profiles obtained by cluster mean field varying n , for $L = 1000$ and $E = -0.8$

Again comparing the CMF and KMC results they are in good agreement, so the theoretical prediction of the existence of a shock phase is confirmed by the numerical simulation (Figure 12), hence cluster mean field is the most suitable approximation to deal with our model, then from now on we will no longer consider simple mean field results.

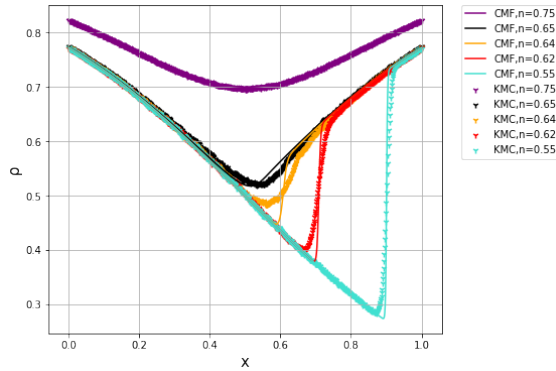


Figure 12: Comparison between $\rho(x)$ profiles obtained by CMF and KMC varying n , for $L = 1000$ and $E = -0.8$

The agreement between CMF and KMC is very good despite for the case $n = 0.64$, and this is due to the size effects: remember indeed that we have considered a system of $L = 1000$ sites, now if we increase L we find that cluster mean field results match kinetic Monte Carlo ones (Figure 13).

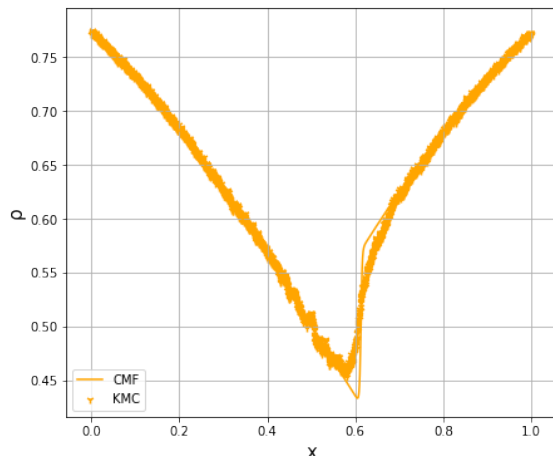


Figure 13: Comparison between $\rho(x)$ profiles obtained by CMF and KMC, for $n = 0.64$, $L = 3200$ and $E = -0.8$

4.2 Features of the steady state when the interaction is strong

Throughout this Section we will show what happens to the steady state of our system when the interaction energy is set at $E = -4$.

This case is representative of a whole range of values of the interaction, strongly repulsive, for which a much more complex phenomenology is obtained with respect to those observed previously.

After the number of sites is set at $L = 1000$ and different values of the average density n are chosen, the CMF algorithm employed to compute the steady state density is let evolve until ζ stays below the threshold 1×10^{-12} - for each value of n - and we are provided with the results shown in Figure 14.

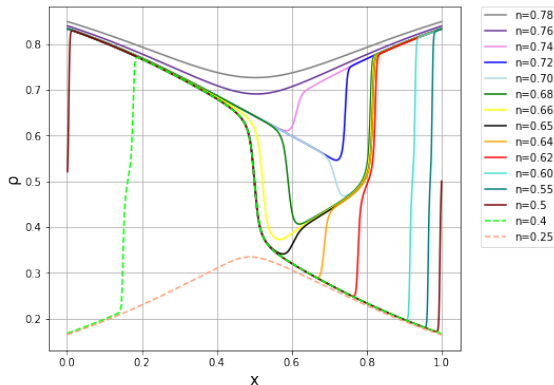


Figure 14: Comparison among $\rho(x)$ profiles obtained by cluster mean field varying n , for $L = 1000$ and $E = -4$

Hence also with bigger interaction strength, when $n \rightarrow 0$ and $n \rightarrow 1$ the steady state of the system corresponds, respectively, to the generalized LD and HD phases.

But for n approaching $1/2$ a new scenario is theoretically predicted by CMF approximation: this time there exist many shock phases, only one of them is characterized by a single shock, while the others have more than one shock.

In particular, looking at Figure 14, cluster mean field results show that when n passes from 0.76 to 0.74 the system undergoes a phase transition to a phase with one shock, then passing from $n = 0.72$ to $n = 0.70$ there is another transition, this time to a phase with two shocks. Furthermore between $n = 0.68$ and $n = 0.66$ a transition to a phase with 3 shocks occurs.

This time there are more phases that can "coexist" with respect to the case with $E = -0.8$, they are: HD phase characterized by $0.65 \lesssim \rho \lesssim 1$, LD one for $0 \leq \rho \lesssim 0.35$ and 2 new phases that are HD_1 and LD_1 characterized by densities slightly above or below 0.5 ($0.5 \lesssim \rho \lesssim 0.65$ and $0.35 \lesssim \rho \lesssim 0.5$ respectively).

Looking at the density profile for $n = 0.72$ in Figure 14 for instance, it is possible to notice that the two "coexisting" phases are HD and HD_1 .

As in the previous cases, increasing the size of the 1D lattice considered in our model, it is possible to notice that the domain walls become more evident, and consequently it is easier to identify which phase characterizes the system, given a certain n (Figure 15).

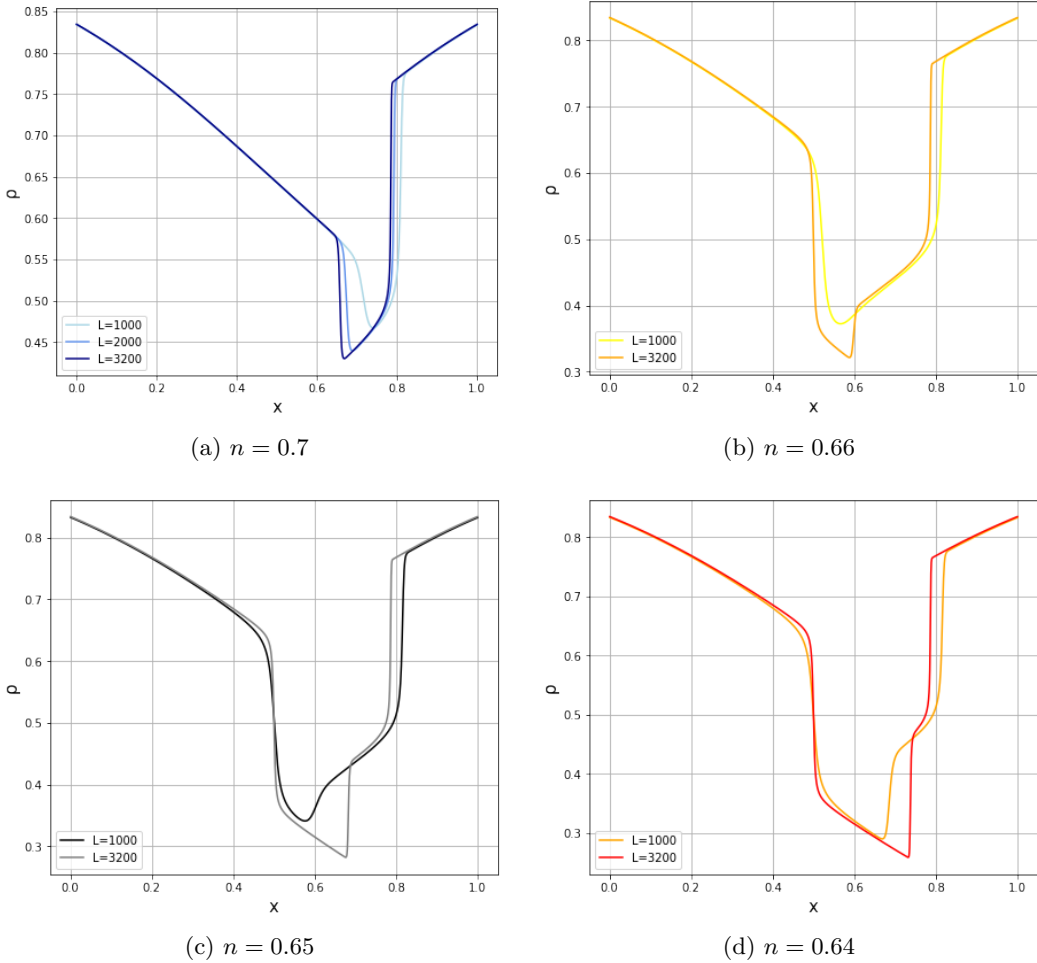


Figure 15: $\rho(x)$ provided by CMF varying L , with interaction energy $E = -4$ and $n = 0.7$, $n = 0.66$, $n = 0.65$, $n = 0.64$ in panels (a),(b),(c),(d) respectively

Looking at panels (a) and (b) in Figure 15, it is possible to say that when the number of lattice sites is 1000: for $n = 0.7$ and $n = 0.66$, the stationary state of our system is a II shock phase, instead for $n = 0.65$ and $n = 0.64$, portrayed in panels (c) and (d), the system is in a III shock phase.

Instead when L increases to 3200 the density profiles stay qualitatively unchanged except for the case $n = 0.66$, in which the stationary state of the system passes from a II shock phase to a III shock phase.

In particular when the average density is equal to 0.7 (for $1000 \leq L \leq 3200$), the stationary state of the system is characterized by phase separation among 3 phases: HD_1 , LD_1 and HD. Besides, if the average density is equal to 0.65 or 0.64 (for $1000 \leq L \leq 3200$) or to 0.66 (for $L = 3200$), there are 3 phases that "coexist": HD, LD_1 and LD. Moreover with $n = 0.66$ (for $L = 1000$) the steady state corresponds to the "coexistence" of 2 phases: HD and LD_1 .

Considering $n = 0.65$ for instance, the steady state is characterized by the "coexistence" of : high density phase for $0 \leq x \lesssim 0.45$ and $0.8 \lesssim x \leq 1$ (recalling that site L equal to site 0 due to the PBC), low density for $0.45 \lesssim x \lesssim 0.65$ and LD_1 for $0.65 \lesssim x \lesssim 0.8$.

In addition it is important to notice that the position of the domain walls (even for the same kind of shock phase) moves as n varies.

Now let us see if the theoretical predictions shown above, are confirmed by numerical simulations (KMC).

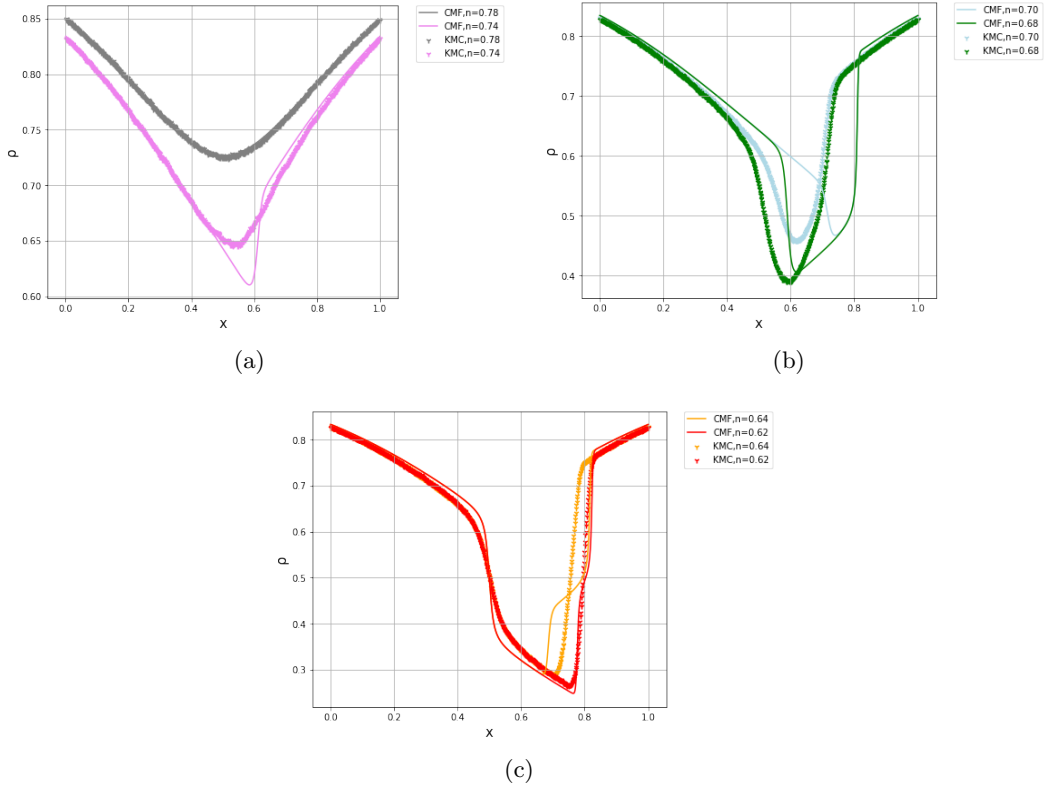


Figure 16: Comparison between $\rho(x)$ profiles obtained by CMF and KMC varying n , for $L = 1000$ and $E = -4$

Figure 16 shows that also density profiles obtained by KMC display more than one domain wall for certain values of n , but not in the same way CMF profiles do. For instance when $n = 0.62$ or $n = 0.64$ cluster mean field $\rho(x)$ has 3 shocks, while kinetic Monte Carlo $\rho(x)$ seems to have only 2 shocks, then if $n = 0.68$ or $n = 0.7$ the density profiles obtained by CMF have 2 shocks, whereas it is not very clear whether the ones obtained by KMC have one or two shocks, furthermore when $n = 0.74$ cluster mean field $\rho(x)$ shows 1 shock, while kinetic Monte Carlo $\rho(x)$ has no shock

Since we have seen in Section 4.1 that, for $E = -0.8$, when CMF and KMC results are not in good agreement it is only a matter of size, we try to increase the number of sites to $L = 3200$ and compare the theoretical and simulated density profiles for $E = -4$ as well.

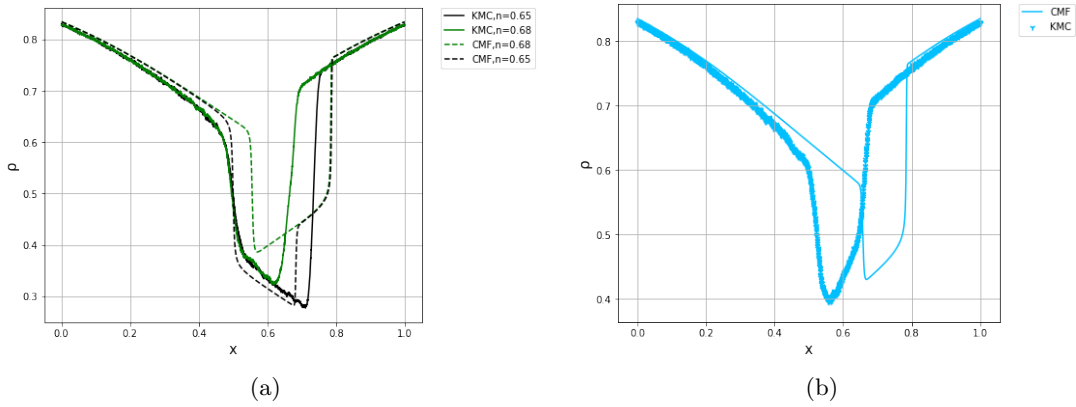


Figure 17: Comparison among $\rho(x)$ profiles obtained by cluster mean field and kinetic Monte Carlo varying n , for $L = 3200$ and $E = -4$. In panel (a) $n = 0.65$ and $n = 0.68$. In panel (b) $n = 0.70$

As illustrated in Figure 17, KMC density profiles are more similar to CMF ones with respect to Figure 16. Indeed, for instance, both for $n = 0.68$ and $n = 0.70$, kinetic Monte Carlo $\rho(x)$ display 2 shocks as predicted by cluster mean field.

So we confirmed with KMC simulations that phases with more than 1 shock do exist in our system.

The analysis done in this thesis has, as a starting point, an article by B. Pal and A.K. Gupta [2], to which we referred in Section 2.2.

However in that article the authors were not able to find, through simulations, the confirmation of the fact that for $E = -4$ there exist phases with more than one shock.

The disagreement they have found between theoretical predictions and numerical simulations, can be due to the fact that they supposed the system to be in the thermodynamic limit, but effectively considered a too small system size.

We show the comparison between our results and theirs in the following Figure 18:

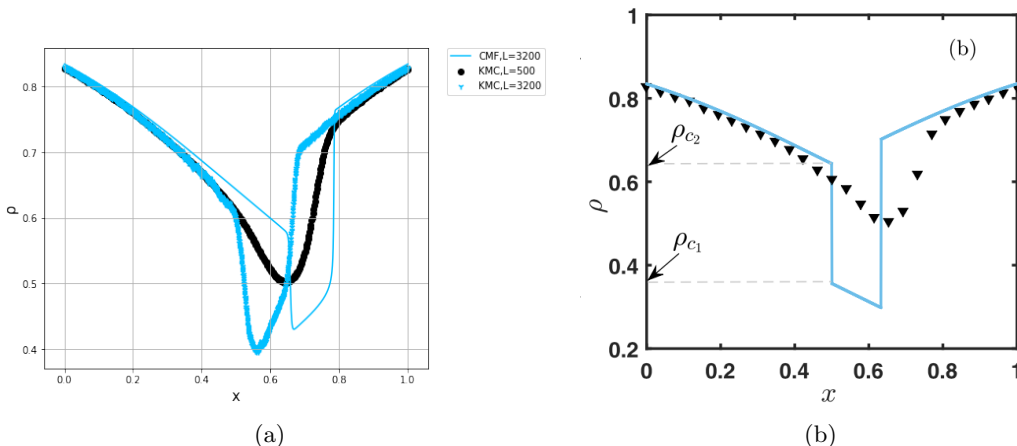


Figure 18: Comparison between $\rho(x)$ profiles obtained by CMF and KMC, for $n = 0.7$ and $E = -4$. In panel (a) our results. In panel (b) [2] results for $L = 500$, KMC $\rho(x)$ is denoted in black, while CMF $\rho(x)$ in blue

As it can be deduced from Figure 18, the possibility to see a phase with more than one shock with KMC, depends on the number of lattice sites we consider.

Besides, notice that the authors of [2], identified ρ_{c1} and ρ_{c2} as the limit densities for the LD and HD phases respectively, without contemplating the existence of intermediate phases (LD_1 and HD_1).

We were not able to observe the 3 shock phase in the KMC simulations. However, since we have seen with CMF that the passage from 2 to 3 shocks can occur due to size effect, it is possible that 3 shock phase actually exists in this model, but can only be observed with very large systems, that it was not possible to simulate in the scope of this thesis.

4.3 Steady state particle current and comparison with analytical solutions

In this Section we will talk about the current of particles at the stationary state and its relation with the phase of the system, then we will compare our finite-size $\rho(x)$ profiles with analytical ones.

When a system reaches the stationary state, by definition the density is constant in time, i.e. $\dot{\rho}_i^t = 0$, this implies that, recalling the continuity equation for our discrete model (13), the particle current J_i is equal to $J_{i+1} \forall i$.

When mean field and cluster mean field methods are employed, the formulas for the particles current J_i^t are respectively (12) and (20), and they are updated - as explained in Section 3.1 - until the steady state is reached. At this point we have L values of J_i (with each method) that are almost identical, hence we take as the value of the current at the steady state the one defined as:

$$J = \frac{\sum_{i=0}^{L-1} J_i}{L} \quad (29)$$

When kinetic Monte Carlo is implemented instead, the current in each site J_i is defined

as the number of times a particle hops in site i per unit time; once obtained $J_i \forall i$, the current at the steady state is obtained through (29) as well.

Notice that using equation (29) in simulations is particularly important because it allows to reduce the statistical uncertainty.

Now we want to compare (Figure 19) the behaviour of the current in systems with interaction energy equal to -0.8 and -4 , computed with the usual methods, for different values of average density.

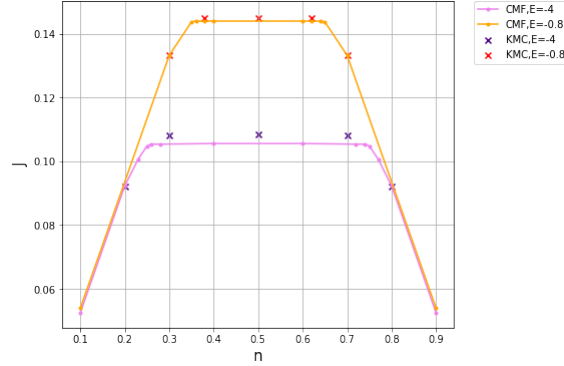


Figure 19: Comparison among $J(n)$ profiles obtained by CMF and KMC, for $E = -0.8, -4$ and $L = 3200$

The qualitative behaviour of the profiles is the same, independently of the interaction energy and the methods: they are symmetric with respect to the axis $n = 0.5$ (particle-hole symmetry), and have a plateau in correspondence of the maximal current (J_{max}). On the other hand the quantitative behaviour strictly depends on the nearest neighbor interaction.

We observe that as $|E|$ increases, the current value related to a certain n decreases and the range of n to which corresponds $J = J_{max}$ becomes wider.

The range of average density values for which J is maximal corresponds to those n for which the stationary state of the system is a shock phase.

This is an interesting result and is a novelty with respect to the scenario described in [2] and illustrated in panel (a) of Figure 20. The authors indeed claimed the existence of a shock phase for which the current is not maximal, instead we have realized that no such phase exists, neither for $E = -0.8$ nor for $E = -4$.

Focusing on panel (b) of Figure 20, it is possible to see that we have obtained $J = J_{max}$, by both KMC and CMF, for $0.36 \lesssim n \lesssim 0.64$ for $E = -0.8$, and for $0.26 \lesssim n \lesssim 0.74$ for $E = -4$. These ranges of n are in fact the ones in which the system is characterized by a shock phase (see Figures 11 and 14).

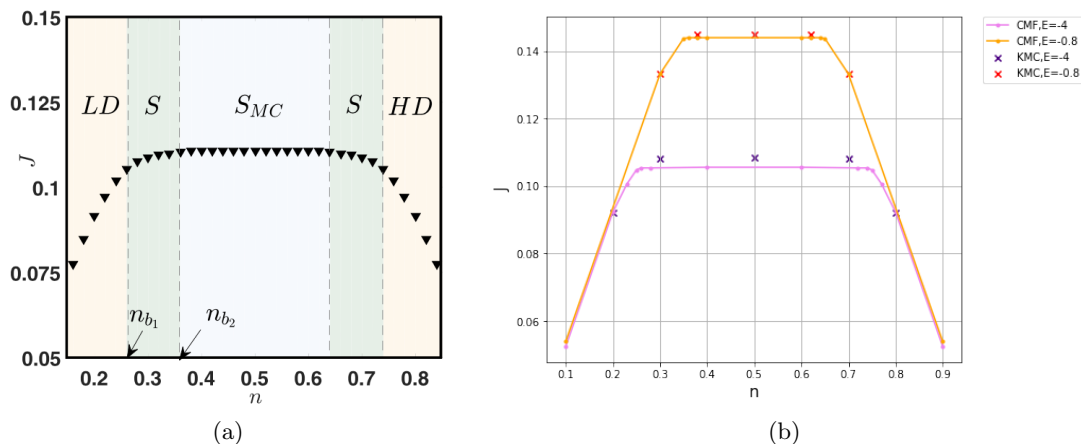


Figure 20: Particle current as a function of the average density. In panel (a) plot obtained in [2] with KMC, $L = 500$ and $E = -4$. In panel (b) our plots obtained by KMC and CMF, $L = 3200$ and $E = -0.8, -4$

In the already cited article [2], the authors derived an analytical equation to compute the cluster mean field current-density relation in the thermodynamic limit:

$$J = \lambda(x) \left(\frac{\sqrt{r^2 + 4r\rho(q-r)(1-\rho)} - r}{4(q-r)^3\rho(\rho-1)} \right) (4r\rho(q-1)(q-r)(\rho-1) + (\sqrt{r^2 + 4r\rho(q-r)(1-\rho)} - r)(2rq - q - r)) \quad (30)$$

Where we recall that we have always considered $\lambda(i/L) = ((i+0.5)/L - 0.5)^2 + 0.5$, for $i = 0, \dots, L-1$.

We are interested in the comparison between the analytical solutions $\rho(x)$ of (30), and the solutions we have obtained at large but finite size, for both $E = -0.8$ and $E = -4$.

4.3.1 Weak interaction

First of all, let us compute the analytical solutions when the current J is maximal. When $E = -0.8$, the factors q and r defined in Section 2.2 are respectively equal to 0.67032 and 1.49182, then independently of the multiplicative factor λ , the qualitative behaviour of $J(\rho)$ is the one in Figure 21:

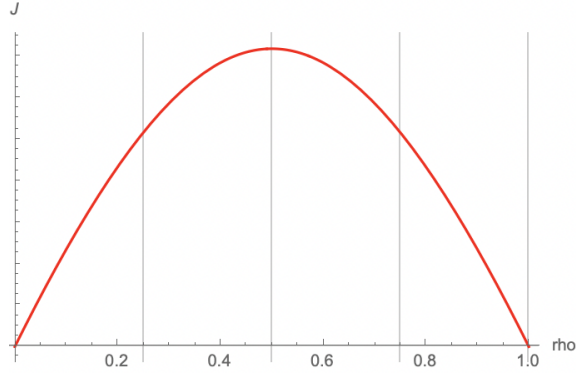


Figure 21: $J(\rho)$ with generic value of λ and $E = -0.8$

J has a single maximum for $\rho = 0.5$. Hence inserting $\rho = 0.5$ and $\lambda = \lambda_{min} = 0.5$ in (30), one obtains $J_{max} = 0.143841$.

Now solving (30) for generic ρ as a function of x , with $J = J_{max} = 0.143841$, it is possible to obtain the solutions shown in Figure 22.

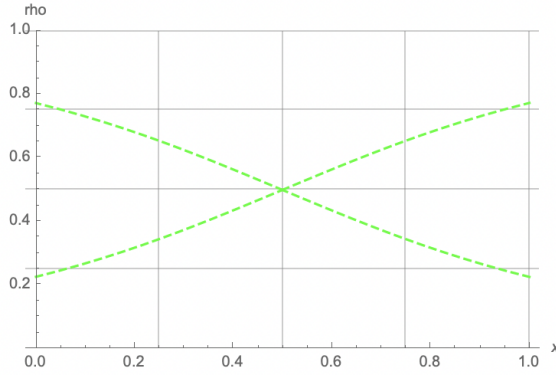


Figure 22: Analytical $\rho(x)$ for $J = J_{max}$ and $E = -0.8$

One solution stays in the upper part of the vertical axis ($1/2 \leq \rho \leq 1$), while the other is in the range $0 \leq \rho \leq 1/2$, and represent the densities in the HD and LD phases respectively.

At this point we compare these solutions with the ones we obtained in Figure 11, for some values of average density (Figure 23). When $n = 0.5$ and $n = 0.62$, the stationary state of the system is the shock phase and indeed our $\rho(x)$ (solid lines), jumps from one solution (dotted line in the lower half of the ρ -axis) corresponding to the LD phase solution, to the other solution (dotted line in the upper half of the ρ -axis), which is the HD phase solution, in correspondence of the domain wall. For $n = 0.5$ the shock is in correspondence of $x \simeq 1$, while for $n = 0.62$ the domain wall is in correspondence of $x \simeq 0.75$.

The system for $n = 0.66$ is in the HD phase, and indeed the values of our ρ stay almost always just above the analytical solution in the upper half of the vertical axis.

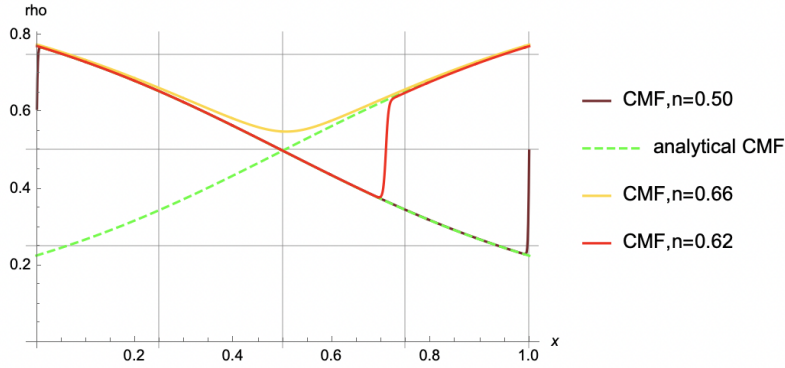


Figure 23: Comparison between analytical (dotted lines) and finite-size $\rho(x)$ (solid lines) solutions for $J = J_{max}$ and $E = -0.8$

Now if we estimate a value of $J < J_{max}$ corresponding to an average density for which the system is not in a shock phase, we observe a different scenario.

For instance computing through CMF the value of the current corresponding to $n = 0.66$ using (29), we get $J = 0.142155$.

This J is an approximation of the current we would obtain from formula (30) once inserted the analytical $\rho(x)$, but it works very well since it is obtained considering a large system size ($L = 3200$).

As Figure 24 shows, for $J = 0.142155$ the finite-size solutions $\rho(x)$ with $n = 0.62$ and $n = 0.5$ match the analytical one in a worse way than before, this is because in this case the value of the current is not maximal, and this is not possible in a shock phase. Whereas the finite-size solution for $n = 0.66$, whose corresponding steady state is not a shock phase and whose current is not maximal, matches better than before the analytical solution with $\rho \geq 1/2$

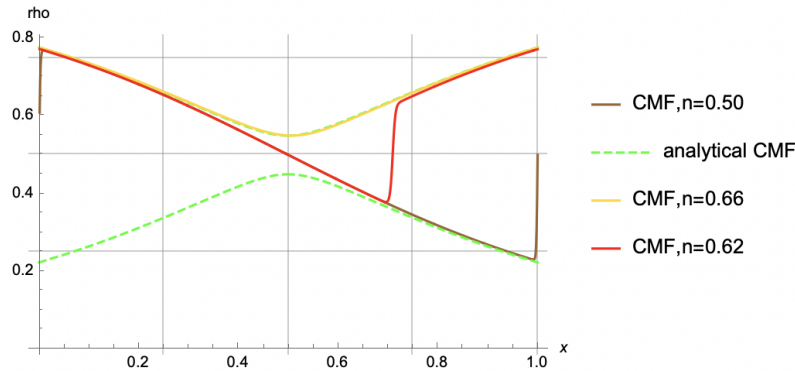


Figure 24: Comparison between analytical (dotted lines) and finite-size $\rho(x)$ (solid lines) solutions for $J = 0.142155 < J_{max}$ and $E = -0.8$

4.3.2 Strong interaction

For $E = -4$, the factors q and r are respectively equal to e^{-2} and e^2 ; the qualitative behaviour of $J(\rho)$, regardless of the value of λ , is the one in Figure 25.

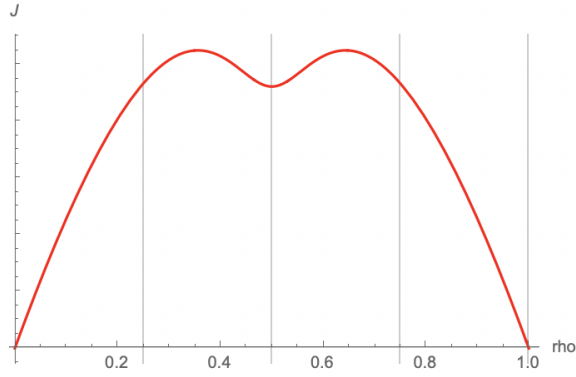


Figure 25: $J(\rho)$ with generic value of λ and $E = -4$

Notice that the current-density relation has 2 lateral (symmetric) maxima, and that J in the current equation (30) depends on ρ only through $I = \rho(1 - \rho)$, hence computing the value of I for which J is maximal, and reminding that $r = 1/q$, one obtains

$$I^* = \frac{1}{2(1+q)} \left(\sqrt{\frac{2}{1-q}} - 1 \right) \quad (31)$$

Then inserting it in (30), we are given the value of the maximal current $J_{max} = 0.105239$. Now solve the current equation setting $J = J_{max}$ (as done before) and the corresponding analytic expression of $\rho(x)$ is the one in Figure 26

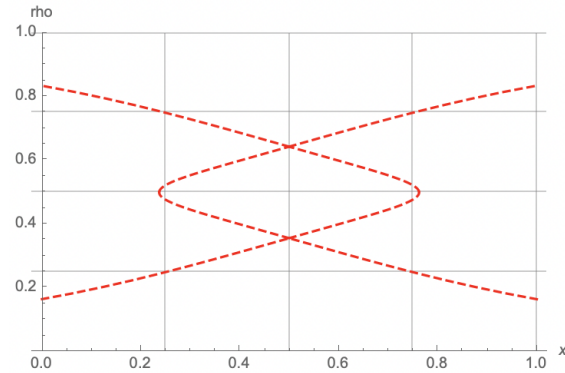


Figure 26: Analytical $\rho(x)$ for $J = J_{max}$ and $E = -4$

Here there are four solutions: starting from $\rho = 1$, and moving towards $\rho = 0$ along the vertical axis, we encounter the density solution characterizing the HD phase for $0.65 \lesssim \rho \lesssim 0.85$, then the one typical of the HD_1 phase for $0.5 \lesssim \rho \lesssim 0.65$, finally the solutions of the LD_1 and LD phases are in the lower half of the rho-axis and correspond to $1 - \rho(x)$ where $\rho(x)$ are the densities in the HD_1 and HD phases respectively.

At this point we compare these solutions with the ones we obtained in Figure 14, for some values of average density (Figure 27). For $n = 0.72$ the system is in a I shock phase, and indeed the finite-size $\rho(x)$ (solid blue line) jumps from the HD_1 to the HD solution (dotted line), for $n = 0.68$ the system is in a II shock phase, and the finite-size density profile (solid orange line) jumps from the HD_1 to LD_1 and then to the HD solution. Moreover when

the stationary state of the system is a III shock phase, for instance with $n = 0.64$, our solution jumps from HD to LD then to LD_1 and eventually to HD phase solution again. When $n = 0.25$ the system is characterized by the low density phase, and our density profile matches quite well the LD analytical solution, however, as seen before, these two solutions are in better agreement when the current is smaller.

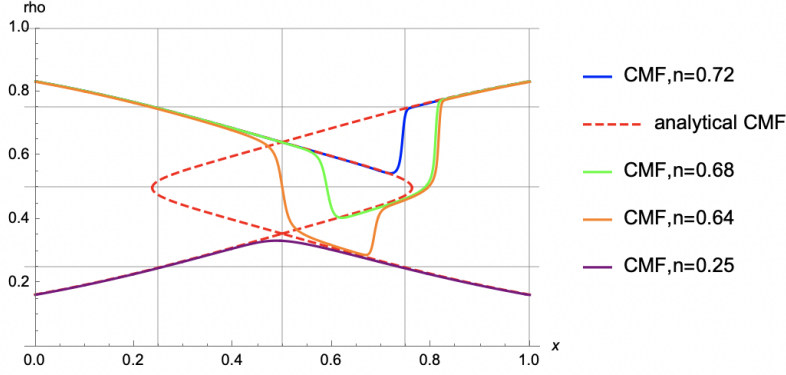


Figure 27: Comparison between analytical (dotted lines) and finite-size $\rho(x)$ (solid lines) solutions for $J = J_{max}$ and $E = -4$

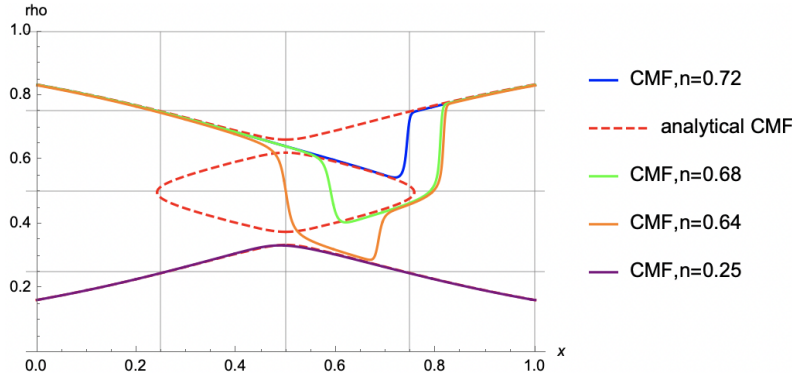


Figure 28: Comparison between analytical (dotted lines) and finite-size $\rho(x)$ (solid lines) solutions for $J = 0.104740 < J_{max}$ and $E = -4$

Indeed, once determined the value of J corresponding to $n = 0.25$ as done in Subsection 4.3.1, it is possible to see (Figure 28) that when the current is not maximal, some portions of our solutions referred to the shock phases do not match the analytical ones (not only in correspondence of the domain wall).

Instead, the finite-size solution for $n = 0.25$ (for which the system is in the LD phase, where $J \neq J_{max}$) is almost identical to the analytical one.

In the end note that we have been able to find 4 distinct solutions, both with finite-size and analytical CMF, while the authors of [2], never found 2 additional solutions (besides HD and LD ones) in the strong repulsion regime.

5 Conclusions and open questions

In this thesis we have considered a model called TASEP which has been proposed in the statistical physics literature to describe transport of interacting particles along a heterogeneous lattice (like biological transport).

In particular we have regarded TASEP model with periodic boundary conditions, quenched hopping rates and interacting nearest neighbour particles and we have studied it with mean field, cluster mean field and kinetic Monte Carlo methods.

We have found that, once fixed the average particles density, both qualitative and quantitative behaviours of the steady state density of a system modeled by TASEP, change depending on the value of the interaction energy.

Taking the same absolute value of the nearest neighbour interaction energy E and changing its sign, density profiles $\rho(x)$ change quantitatively (see Figures 5, 6 and 8), conversely varying $|E|$, the density profiles change also qualitatively (compare Figures 11 and 14).

In particular we have seen (also through KMC simulations) that increasing the strength of the repulsion between nearest neighbour particles, from $E = -0.8$ to $E = -4$, the shock phase passes from having only one shock to the possibility of having a maximum of 3 shock. This result had never been observed before through numerical simulations.

The existence of phases with more than one shock, confirmed by numerical simulations, is the most important novel result of this thesis, and represents a step forward with respect to the work done so far about TASEP model with non uniform (quenched) hopping rates and local interactions.

In particular we have been able to improve some results obtained in [2]: there the authors did not realize the existence of new phases in presence of a strong repulsive interaction, whereas we have found 2 new phases: LD_1 and HD_1 . Moreover, based on this result, we have solved the discrepancies between CMF and KMC outcomes in [2], which has also required to significantly increase the system size in our simulations.

By the way we have also noticed that, due to the large finite-size effects, the authors of [2] wrongly predicted that a shock phase could appear even without maximal current.

Conversely, we have verified that when the stationary state is a shock phase, it is always characterized by the maximal current for such system.

This result has been already achieved in the article [10], in which interactions were not considered though. The authors explained it in the following way: as n increases from 0 the current J increases until it reaches its maximal value J_{max} , in the meanwhile the system stays in the LD phase. When $J = J_{max}$ the HD and LD solutions coincide at $x = 0.5$ that is the value for which $\lambda(x)$ is minimal (look at Figures 22 and 26), hence for increasing n the additional particles go over the HD solution. At this point since the system is closed the solution has to return on the LD one and it does this through a jump, the domain wall.

In addition the position of the shock moves as n raises to "make the region of existence for HD solution larger and for LD smaller".

We have focused our analysis only on systems with negative interaction energy between particles, because the scenario for attractive interaction turns out to be less interesting. Indeed even for considerable variations of the attractive energy strength, the system settles in a smooth phase or at most in a I shock phase (look at panel (a) of Figure 29).

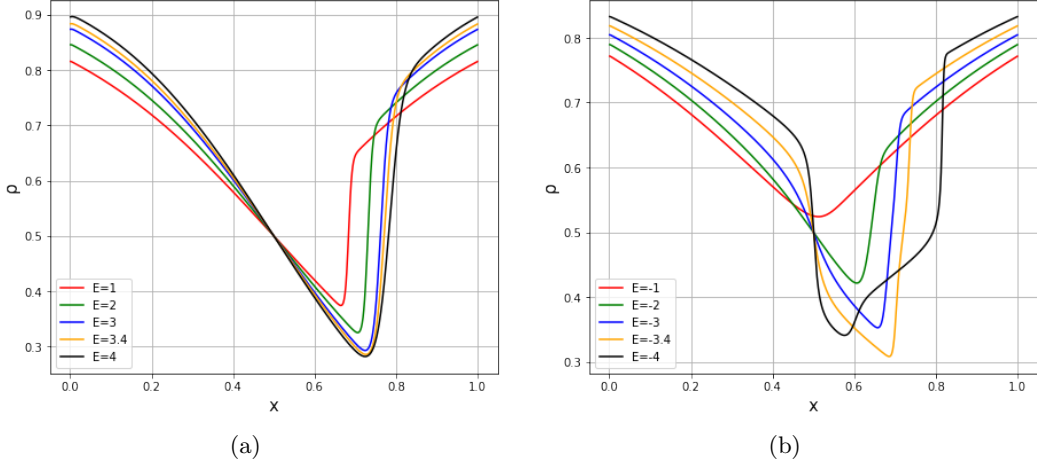


Figure 29: Density profiles obtained with CMF for average density $n = 0.65$ and $L = 1000$, with positive E in panel (a) and negative E in panel (b)

This behaviour is qualitatively similar to the one already observed in [10] where interactions were not present.

On the contrary for the very same average densities, when the negative interaction energy ranges from -4 to -8 the scenario is very different: as portrayed in panel (b) of Figure 29 the steady state is firstly in a smooth phase, then it is in a shock phase characterized by a number of shocks that increases as $|E|$ increases.

At this point we wonder how the number of shocks varies as the absolute value of the energy varies over a wider range.

It may happen that decreasing the strength of the repulsive interaction, the maximum number of shocks in the shock phases decreases. Similarly, maybe increasing the repulsive energy, there will be shock phases with an increasing number of shocks.

To investigate this issue we have created many plots of $\rho(x)$ through CMF, varying the average density and the repulsive energy, and we have distinguished among the cases in which the stationary state of the system would be in a phase without shocks or in a phase with one, two, three (or more) shocks, hence we have placed the results in the phase diagram sketched in Figure 30. (Note that we have limited our description only to $0.5 \leq n \leq 1$, because the picture for $0 \leq n \leq 0.5$ is the symmetric of this one due to particle-hole symmetry).

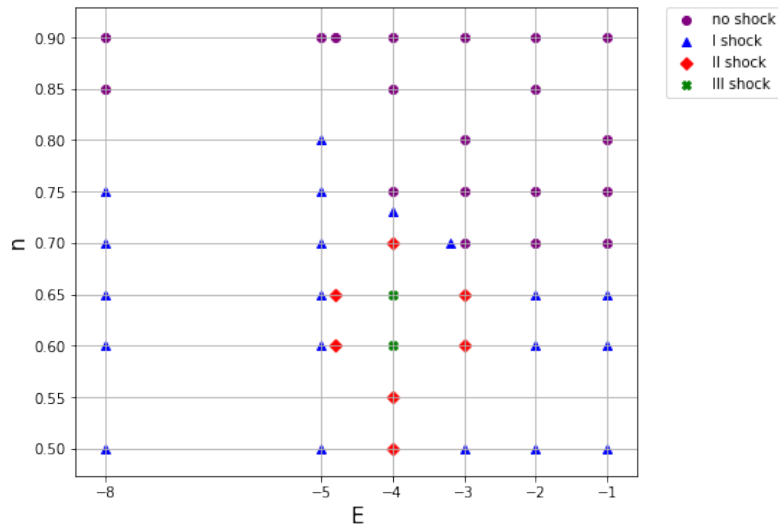


Figure 30: Phase diagram of our system depending on n and E (results obtained for $L = 1000$)

We never observe a steady state characterized by more than 3 domain walls, and moreover, whenever a transition occurs, it is between a phase with k shocks and another phase with $k + 1$ or $k - 1$ shocks, for $k = \{1, 2\}$.

Even though our analysis of the phase diagram is still quite rough and incomplete, we are quite confident about our observations.

It would be interesting to confirm the above theoretical predictions also with KMC simulations, which is something that we have not been able to do in this thesis because of the too long computational time required.

However, due to the good agreement that we have observed throughout this thesis between CMF results and KMC simulations, we are quite confident that even these last predictions are correct.

Furthermore we expect that the CMF method could be a valuable tool to investigate other TASEP-like models, possibly more detailed and realistic for applications.

References

- [1] Chowdhury D., Schadschneider A. and Nishinari K. "Traffic phenomena in biology: from molecular motors to organisms". *Traffic and Granular Flow'05*, **223-238** (2007).
- [2] Pal B. and Gupta A. K. "Role of interactions in a closed quenched driven diffusive system". *Journal of Physics A: Mathematical and Theoretical* **54**, 025005 (2020).
- [3] Teimouri H., Kolomeisky A. B. and Mehrabiani K. "Theoretical analysis of dynamic processes for interacting molecular motors". *Journal of Physics A: Mathematical and Theoretical* **48**, 065001 (2015).
- [4] Celis-Garza D., Teimouri H. and Kolomeisky A. B. "Correlations and symmetry of interactions influence collective dynamics of molecular motors". *Journal of Statistical Mechanics: Theory and Experiment* **2015**, P04013 (2015).
- [5] Botto D., Pelizzola A., and Pretti M. "Dynamical transitions in a driven diffusive model with interactions". *EPL (Europhysics Letters)* **124**, 50004 (2018).
- [6] Pelizzola A. and Pretti M. "Cluster approximations for the TASEP: stationary state and dynamical transition". *The European Physical Journal B* **90**, 1-8 (2017).
- [7] Pelizzola A., Pretti M. and Puccioni F. "Dynamical Transitions in a One-Dimensional Katz–Lebowitz–Spohn Model". *Entropy* **21**, 1028 (2019).
- [8] Gillespie, D. T. "Exact stochastic simulation of coupled chemical reactions." *The journal of physical chemistry* **81**, 2340-2361 (1977).
- [9] Schadschneider A., Chowdhury D., Nishinari K. "Stochastic transport in complex systems from Molecules to Vehicles". Elsevier Science (2010).
- [10] Banerjee T. and Basu A. "Smooth or shock: Universality in closed inhomogeneous driven single file motions". *Physical Review Research* **2**, 013025 (2020).